Protein Structure and Folding:

NMR Solution Structure of Human Vaccinia-related Kinase 1 (VRK1) Reveals the C-terminal Tail Essential for Its Structural Stability and Autocatalytic Activity

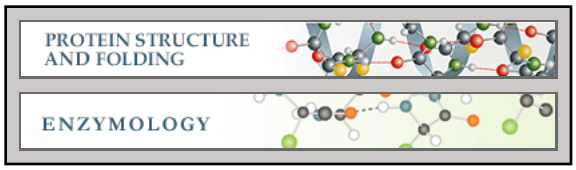

Joon Shin, Goutam Chakraborty, Nagakumar Bharatham, CongBao Kang, Naoya Tochio, Seizo Koshiba, Takanori Kigawa, Wanil Kim, Kyong-Tai Kim and Ho Sup Yoon

J. Biol. Chem. 2011, 286:22131-22138.
doi: 10.1074/jbc.M110.200162 originally published online May 3, 2011

THE JOURNAL OF BIOLOGICAL CHEMISTRY VOL. 286, NO. 25, pp. 22131–22138, June 24, 2011

NMR Solution Structure of Human Vaccinia-related Kinase 1 (VRK1) Reveals the C-terminal Tail Essential for Its Structural Stability and Autocatalytic Activity*[S]

Received for publication, November 3, 2010, and in revised form, April 20, 2011 Published, JBC Papers in Press, May 3, 2011, DOI 10.1074/jbc.M110.200162

Joon Shin[‡1], Goutam Chakraborty[‡1], Nagakumar Bharatham[‡], CongBao Kang[‡2], Naoya Tochio[§], Seizo Koshiba[§], Takanori Kigawa[§], Wanil Kim[¶], Kyong-Tai Kim[¶], and Ho Sup Yoon[‡3]

From the [‡]School of Biological Sciences, Nanyang Technological University, Singapore 637551, the [§]RIKEN Systems and Structural Biology Center, Yokohama 230-0045, Japan, and the [¶]Department of Life Science, Pohang University of Science and Technology, Pohang 790-784, Republic of Korea

Vaccinia-related kinase 1 (VRK1) is one of the mitotic kinases that play important roles in cell cycle, nuclear condensation, and transcription regulation. Kinase domain structures of two other VRK family members (VRK2 and VRK3) have been determined previously. However, the structure of VRK1, the most extensively studied and constitutively active VRK member, is yet to be characterized. Here, we present the nuclear magnetic resonance (NMR) solution structure of a catalytically active form of human VRK1 with its extended C-terminal tail (residues 1–361). The NMR structure of human VRK1 reveals that the C-terminal tail orients toward the catalytic site and forms a number of interactions that are critical for structural stability and catalysis. The role of this unique C-terminal tail was further investigated by deletion mutant studies where deletion of the terminal tail resulted in a dramatic reduction in the autocatalytic activity of VRK1. NMR titration studies carried out with ATP or an ATP analog confirm that ATP/ATP analogs interact with all of the crucial residues present in important motifs of the protein kinase such as the hinge region, catalytic loop, DYG motif, and thereby suggest that the catalytic domain of VRK1 is not atypical. In addition to the conventional interactions, some of the residues present on the extended C-terminal tail also interact with the ligands. These observations also substantiate the role of the extended C-terminal tail in the biological activity of VRK1.

The coordinated action of protein kinases and phosphatases plays a major role in regulating signal transduction events in a multicellular organism (1–3). Kinases comprise one of the major members of the human genome (4), characterized by the presence of a conserved catalytic domain of approximately 300 amino acids which is involved in the phosphotransfer reactions (5–7). Vaccinia-related kinase 1 (VRK1)[4] belongs to a novel group of serine/threonine kinases that bear a high degree of sequence similarity with vaccinia virus B1 R kinase (8, 9). Three members of VRK family are known in the human genome and show a significant sequence similarity among themselves with respect to their catalytic domains, but differ in their regulatory domains (8, 10). VRK1 is the most well studied member of the family, known to participate in a number of biological activities especially in cellular proliferations as well as in management of cellular stress situations (11). A number of studies demonstrated that VRK1 phosphorylates several stress-related transcription factors *e.g.* p53, c-Jun, ATF2, which in turn play a major role in regulating cellular fate (10–12).

Several studies have also reported the role of VRK1 in cellular proliferation both in normal cells as well as in cells with uncontrolled proliferation (13). Elevated levels of VRK1 protein have been observed in highly proliferative cell lines, indicating its role in cell division (14). Furthermore, VRK1 is a nuclear protein, known to play an important role in cell cycle progression through phosphorylation of barrier to autointegration factor (15–17), which helps in formation of the nuclear envelope during cell division (18, 19) and in the chromatin condensation event during cell division by phosphorylating histone H3 both at threonine 3 and serine 10 residues (20, 21).

The catalytic domain structures of VRK2 and VRK3 reveal the typical kinase fold but with a degraded catalytic site on VRK3 (22). It is noted that the catalytic domains of VRKs are flanked by the large noncatalytic regions either at N or C termini. VRK1 contains a C-terminal noncatalytic tail but is constitutively active. Currently, the underlying molecular mechanism of VRK1 activation is unknown. In this report, we present NMR solution structures of a catalytically active form of human VRK1 with the C-terminal noncatalytic fragment flanking the

* This work was supported in part by National Medical Research Council of Singapore Grant NMRC/1177/2008; grants from the Core Research Program/Anti-aging and Well-being Research Center; the Brain Korea 21 program of the Ministry of Education, Science, and Technology; and National Research Foundation of Korea Grants 20090063547 and 20090081464 (the Original Technology Research Program for Brain Science).

[S] The on-line version of this article (available at http://www.jbc.org) contains supplemental Figs. S1–S6 and Table 1.

The atomic coordinates and structure factors (code 2LAV) have been deposited in the Protein Data Bank, Research Collaboratory for Structural Bioinformatics, Rutgers University, New Brunswick, NJ (http://www.rcsb.org/).

[1] Both authors contributed equally to this work.

[2] Present address: Experimental Therapeutics Centre, 31 Biopolis Way, Nanos, 03-01, Singapore 138669.

[3] To whom correspondence should be addressed: School of Biological Sciences, Nanyang Technological University, 60 Nanyang Dr., Singapore 637551. Tel.: 65-6316-2846; Fax: 65-6791-3856; E-mail: hsyoon@ntu.edu.sg.

[4] The abbreviations used are: VRK, vaccinia-related kinase; AMP-PCP, adenosine 5′-(β,γ-methylenetriphosphate); HSQC, heteronuclear single quantum coherence; PDB, Protein Data Bank; RDC, residual dipolar coupling; r.m.s.d., root mean square deviation; TOCSY, total correlation spectroscopy; TROSY, transverse relaxation-optimized spectroscopy.

kinase domain, and we propose a molecular basis underlying the activation mechanism of VRK1.

EXPERIMENTAL PROCEDURES

Cloning, Expression, and Purification of the Wild Type and Deletion Mutants of Human VRK1 Protein—The complementary DNAs (cDNAs) encoding the full-length human VRK1 and the C-terminal truncation mutants ($VRK1_{1-391}$, $VRK1_{1-381}$, $VRK1_{1-371}$, $VRK1_{1-361}$, $VRK1_{1-351}$, $VRK1_{1-341}$, $VRK1_{1-331}$) were PCR-amplified using the corresponding forward and reverse primers containing NdeI and XhoI restriction enzyme cleavage sites. The resultant amplified products were gel-purified, digested using the restriction enzymes, and cloned into pET-29b plasmid (Novagen). For the protein purification, cells were grown in M9 medium containing $^{15}NH_4Cl$, $^{15}NH_4Cl$ plus [U-^{13}C]glucose, and 75% or 100% ^2H_2O at 37 °C at 220 rpm until the culture optical density reached an absorbance of 0.7 at 600 nm. The culture was then induced with 1 mM isopropyl-thio-β-D-galactopyranoside at 25 °C for 4 h. After the cultured cells were harvested by centrifugation, the cell pellet was resuspended in a lysis buffer (20 mM phosphate buffer, pH 7.8, 500 mM NaCl, 1 mM phenylmethylsulfonate, lysed by sonication, and purified on a Ni^{2+}-nitrilotriacetic acid-agarose column (Invitrogen). The eluted proteins from the Ni^{2+}-nitrilotriacetic acid-agarose column were analyzed by 12.5% SDS-PAGE. The fractions containing VRK1 were collected, concentrated, and further purified on a Superdex S-200 column (GE Healthcare) preequilibrated with a buffer containing 20 mM Tris-HCl, pH 6.8, 2 mM dithiothreitol (DTT), and 0.01% NaN_3. The purified proteins were verified by mass spectroscopy at Nanyang Technological University Proteomics Core Facility.

Nuclear Magnetic Resonance (NMR) Data Acquisition and Assignments—Samples for NMR experiments contained 0.3–0.6 mM protein in 20 mM Tris-HCl, pH 6.8, 2 mM DTT, 0.01% NaN_3, and 10% or 100% D_2O. For backbone assignments, transverse relaxation-optimized spectroscopy (TROSY)-based HNCACB, HN(CO)CACB, HNCA, HN(CO)CA, HNCO, and HN(CA)CO spectra were obtained using 100% fully deuterated and uniformly $^{13}C/^{15}N$-labeled VRK1 (23). For side chain resonance assignments, TROSY-based ^{15}N-edited NOESY, HCCH TOCSY, and ^{13}C-edited NOESY experiments using fully or 75% perdeuterated protein samples were performed. Selectively labeled NMR samples on $^{13}C/^{15}N$-labeled valine/isoleucine/leucine residues were prepared, and HCCH TOCSY and ^{13}C-edited NOESY experiments were performed for assignments of side chain methyl resonances and deriving methyl-methyl or methyl side chain distance constraints. NMR experiments were performed on Bruker Avance 700, 800, and 900-MHz spectrometers equipped with a 5-mm triple resonance, *z* axis-gradient cryogenic probe at 298 K. A list of the NMR experiments is shown in supplemental Table 1. All spectra were processed with NMRPipe (24) and analyzed using SPARKY (25). The assigned chemical shift values of VRK1 have been deposited in the Biological Magnetic Resonance Bank (accession code 16738). Residual dipolar couplings (RDCs) were measured using polyethylene glycol/alcohol mixtures (26). 50 μl of C12E5 was mixed in 530 μl of NMR buffer containing 90% H_2O and 10% D_2O for stock solution preparation. 1-Hexanol was gradually added by 2-μl increments with vigorous shaking to a final molar C12E5:1-hexanol ratio of 0.96. After 1 h at room temperature, air bubbles were removed by centrifugation at 5000 × *g* for several minutes. For the measurement of RDCs, 300 μl of the C12E5:1-hexanol stock solution was added to 200 μl of protein. The final concentration of C12E5:1-hexanol mixture in the NMR sample was about 5% (w/w). ^{15}N-^1H RDC constants were measured using combination of ^1H-^{15}N HSQC and ^1H-^{15}N TROSY-HSQC experiments at 25 °C as described previously (27). The data analysis and calculation of alignment tensor were performed using REDCAT software (28) (see supplemental Fig. S6).

NMR Titration of VRK1 with ATP/ATP Analog—Molecular characteristics of ATP/ATP analog binding with VRK1 were studied using two-dimensional TROSY-HSQC spectra of ^{15}N-labeled VRK1 recorded on a Bruker Avance 700 spectrometer at 298 K, and the ligand binding sites were mapped by analyzing chemical shift perturbations. Initially, the NMR spectra of free sample was recorded using 0.1 mM ^{15}N-labeled $VRK1_{1-316}$. The ligands were then added to the sample, and chemical shifts were compared before and after the addition of the ligand.

Structure Calculation and Refinement—Solution structures of VRK1 were calculated by simulated annealing in torsion angle space with combination of the program CYANA 2.1 (29) and CNS 1.2 (30, 31). Distance constraints were derived by analyzing TROSY-based ^1H-^{15}N NOESY (80-ms mixing time) and ^{13}C-edited NOESY (100-ms mixing time) spectra of 50% random fractional deuterated or selective labeled (valine, isoleucine, and leucine residues) samples of VRK1. The secondary structure was predicted by program TALOS+ (32) based on the analysis about sequential ($|i-j| = 1$), short range ($|i-j| < 5$) NH-NH and NH-aliphatic contacts on ^{15}N TROSY-NOESY spectrum. Dihedral angle (ϕ, ψ) restraints were also calculated from chemical shifts using TALOS+, and hydrogen bond restraints were obtained based on protein structure during structure calculations. Manually assigned NOE constraints were classified based on their intensities and applied with upper distance limit of 3.0 Å (strong), 3.5 Å (medium), 5.0 Å (weak), 6.0 Å (very weak), and total 200 conformers were generated as initial structures by CYANA 2.1 from 5193 NOE constraints. An additional 0.5 Å was added for NOEs involving methyl groups. After calculation, initial conformers were sorted by target function values, and the lowest 100 conformers were selected for further refinement using CNS 1.2. 292 backbone hydrogen bonds were identified on the basis of initial structures, and 457 torsion angle constraints derived from chemical shift values with the program TALOS+ were applied in refinement stage. Also, 234 ^{15}N-^1H residual dipolar coupling restraints were included in the final stage of calculation. The final structure was refined by using a simulated annealing protocol with combination of torsion angle space and Cartesian coordinate dynamics as published previously (33). Finally, 20 structures were selected by their total energy values for display and structural analysis. MOLMOL (34) and PyMOL (35) programs were used for structure visualization. The 20 NMR ensemble structures have been deposited in Protein Data Bank (PDB) with code 2LAV.

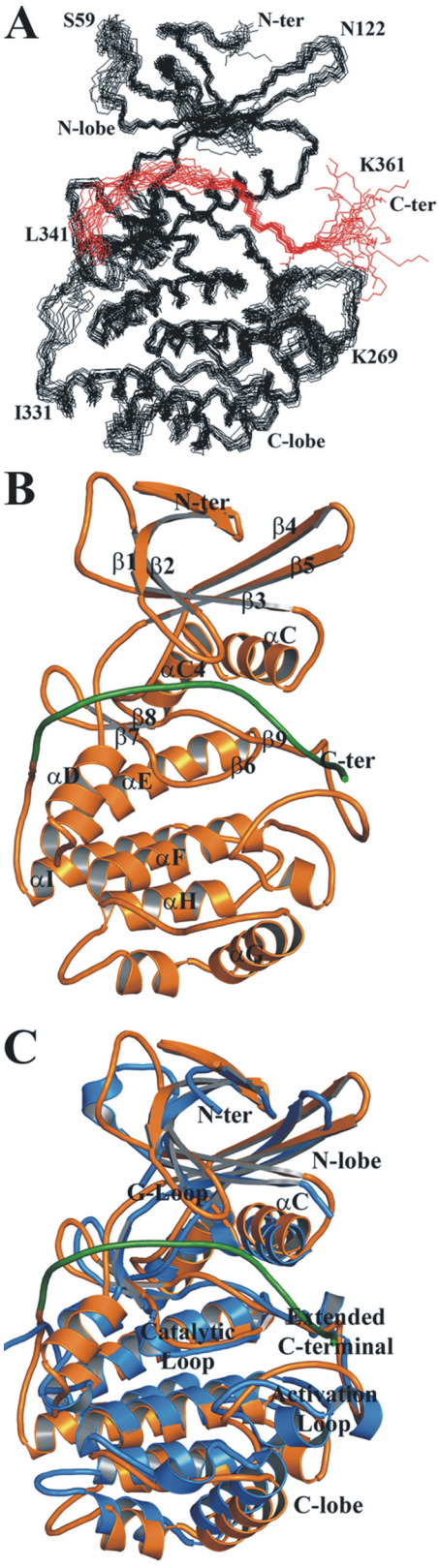

FIGURE 1. **Solution structure of human VRK1.** *A*, superposition of the backbone traces from the final ensemble of 20 solution structures of VRK1 determined by NMR spectroscopy (residues 21–361). The extended C-terminal tail (341–361) is highlighted in *red*. *B*, *ribbon diagram* of VRK1 NMR structure shown in *orange* and the secondary structural elements of VRK1 labeled as indicated. The extended C-terminal tail is highlighted in *green*. *C*, superimposition of VRK1 solution structure (*orange*) and VRK2 structure (*blue*) (PDB 2V62). The r.m.s.d. value for 276 C^{α} atoms between VRK1 NMR and VRK2 structures is 2.56 Å.

TABLE 1
Structural statistics of NMR structures of VRK1

Factors	Without RDC	With RDC
No. of NOE constraints		
All	5193	5193
Intraresidues, $\|i-j\| = 0$	1070	1070
Sequential, $\|i-j\| = 1$	1327	1327
Medium range, $1<\|i-j\|<5$	986	986
Long range, $\|i-j\| >= 5$	1810	1810
No. of hydrogen bond constraints	292	292
No. of dihedral angle constraints	457	457
No. of RDC constraints ($^1D_{NH}$)		234
No. of constraint violations (>0.5 Å)	0	0
No. of angle violations (>5°)	0	0
No. of RDC violations (>1.0 Hz)		0
Parameters for experimental RDC constraints		
*D*a,Hz		2.83
R(rhombicity)		0.13
Q factor[a]		0.12
r.m.s.d. for residue 21–355 to mean[b]		
Backbone	1.68 ± 0.31 Å	1.24 ± 0.18 Å
Heavy atoms	2.36 ± 0.31 Å	1.95 ± 0.23 Å
r.m.s.d. for secondary structural elements to mean[b]		
Backbone	1.19 ± 0.23 Å	0.87 ± 0.13 Å
Heavy atoms	1.85 ± 0.23 Å	1.51 ± 0.17 Å
Ramachandran plot[c]		
Most favored regions	76.3%	76.1%
Additionally allowed regions	20.1%	20.0%
Generously allowed regions	2.3%	2.9%
Disallowed regions	1.3%	1.0%

[a] Q factor was calculated using following formula: r.m.s. $(D^{calc} - D^{obs})$/r.m.s. (D^{obs}), where D^{calc} and D^{obs} are calculated and observed RDC values, respectively.
[b] No. of structures used in r.m.s.d. calculation was 20.
[c] Ramachandran analysis was performed using PROCHECK-NMR program (37).

In Vitro Kinase Assay—The wild-type human VRK1 and its C-terminal truncation mutants were evaluated for their autophosphorylation activity according to the protocol described previously (36). Briefly, 1 μg of the recombinant proteins were placed in a reaction mixture containing 20 mM Tris-HCl, pH 7.5, 150 mM KCl, 5 mM $MgCl_2$, 0.5 mM DTT, 5 μM ATP, and 5 μCi of [γ-^{32}P]ATP. The reaction mixture was then incubated at 37 °C for 30 min. The protein mixtures were resolved by 12% SDS-PAGE. The gels were then exposed to x-ray film overnight and developed using X-OMAT2000 (Kodak).

RESULTS AND DISCUSSION

NMR Solution Structures of VRK1—The structural studies were performed on a catalytically active form of human VRK1 (residues 1–361) lacking 35 residues at C terminus. The structures were determined based on a total of 5193 nontrivial NMR-derived distance restraints and 234 ^{15}N-^{1}H RDC restraints, which were included in the final step of structure calculation. The ensemble of 20 low energy structures calculated with CNS is shown in Fig. 1*A*. Excluding the N-terminal 20 residues and C-terminal 6 residues, the average root mean square deviation (r.m.s.d.) values relative to the mean coordinate of 20 conformers were 1.24 Å for the backbone atoms and 1.95 Å for all heavy atoms. Structural statistics for the NMR ensemble are given in Table 1. There are no distance violations greater than 0.5 Å or dihedral angle violations greater than 5°. Analysis of the average minimized structures with PROCHECK-NMR (37) showed that 76.2% and 20.0% of residues lie in the most favored and allowed regions, respectively.

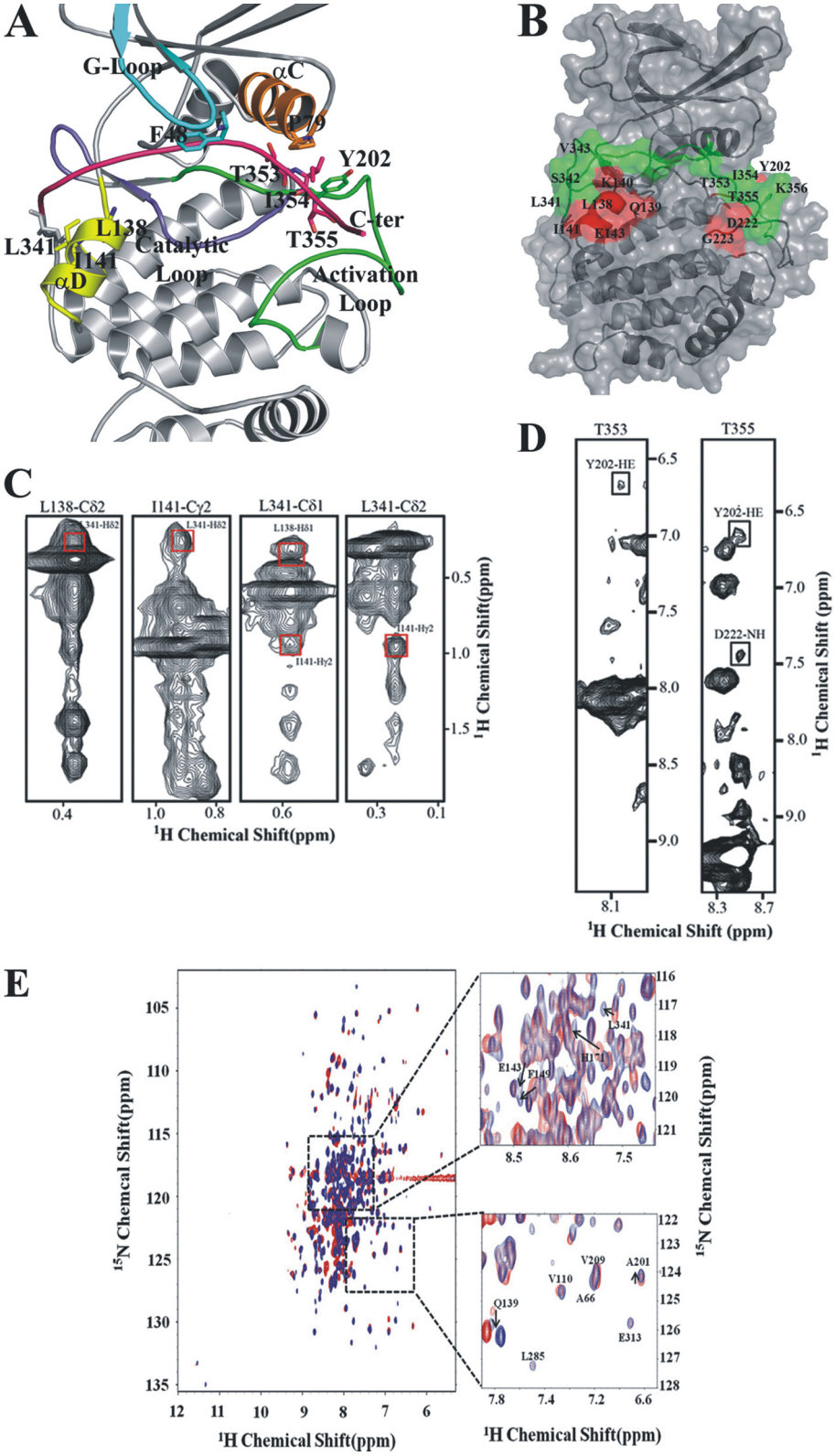

FIGURE 2. **Molecular interaction between the C-terminal tail and the kinase domain.** *A*, extended C-terminal tail interacting with the catalytic core highlighted with *colors*. Crucial hydrophilic and hydrophobic interaction forming residues are shown with *sticks*, and hydrogen bonds are indicated as *dashed lines*. Important regions are highlighted with *colors*: *cyan* (G-loop), *orange* (αC), *blue* (catalytic loop), *green* (activation loop), *yellow* (αD), and *magenta* (C-terminal loop). *B*, interaction site mapping between the central domain and C-terminal extension of VRK1 based on the results of ^{1}H-^{15}N TROSY-HSQC data. Residues in the C-terminal extension are highlighted in *green*; residues affected by C-terminal deletion are indicated in *red*. *C*, representative strips of the ^{13}C-edited three-dimensional NOESY spectrum of VRK1 showing NOE cross-peaks between residues on the αD helix (Leu^{138}, Ile^{141}) and the C-terminal extension (Leu^{341}). *D*, representative strips of the ^{15}N-edited three-dimensional NOESY spectrum of VRK1 showing NOE cross-peaks between residues on the activation loop (Tyr^{202}, Asp^{222}) and the C-terminal extension (Thr^{353}, Thr^{355}). *E*, overlay of ^{15}N TROSY-HSQC spectra of 0.2 mM ^{15}N-labeled VRK1$_{1-361}$ (*red*) and VRK1$_{1-341}$ (*blue*) deletion mutant. Sections of peaks perturbed by C-terminal deletions are also shown on the *right side* of the panel.

The NMR structures of VRK1 reveal the well defined typical kinase fold. The overall fold of the kinase domain of VRK1 is similar to two other VRK kinase members (VRK2 and VRK3) adopting a bilobate structure (Fig. 1). The N-terminal tail (residues 1–20) is unstructured in solution as evidenced by the lack of medium and long range nuclear Overhauser effects (NOEs) in this region. The characteristic additional helix (αC4) is inserted between αC and β4 as predicted. The last helix in the C-terminal lobe (αI) of VRK1 (316–331) is more extended compared with VRK2 and stabilizes the entire protein conformation by forming hydrophobic spines with side chains of aliphatic and aromatic residues present in the protein core (Fig. 1*B*). Most notable and unique feature of the VRK1 solution structure is that the C-terminal tail (residues 341–361) orients around the catalytic site and forms a number of interactions with several important motifs such as G-loop, αC, the catalytic and activation loops (Fig. 1*C* and supplemental Fig. S1).

The C-terminal Tail Interacts with the Catalytic Core and Shows That It Is Essential for VRK1 Structure and Catalysis—The C-terminal tail of VRK1 shows a high degree of sequence conservation across species (8), suggesting its potential regulatory role. The VRK1 NMR structures reveal that Ile^{354} interacts with Pro^{79} of αC, and the residues of αD helix (Leu^{138} and Ile^{141}) also form hydrophobic interactions with Leu^{341} and Val^{343} of the extra C-terminal tail (Fig. 2*A*). The residue Leu^{349} at the C-terminal tail forms a hydrophobic interaction with Phe^{48} of the G-loop. We have investigated the role of the C-terminal tail on VRK1 stability and catalysis by performing chemical shift perturbation experiments on the uniformly ^{15}N-labeled VRK1$_{1-361}$, which was used in our NMR structure determination and VRK1$_{1-341}$ construct where residues 342–361 were truncated. The two-dimensional ^{1}H-^{15}N HSQC spectra of VRK1$_{1-361}$ and VRK1$_{1-341}$ showed noticeable chemical shift perturbations on some of the residues in the activation (Ala^{201}, Tyr^{202}) and catalytic loops (Glu^{172}, Val^{174}, Lys^{179}, Ser^{181}) after the removal of the C-terminal 20 residue extension (Fig. 2*E* and supplemental Fig. S2). In addition, the residues from αD (Leu^{138}–Lys^{140}, Glu^{143}) and the loop connecting αD and αE (Ala^{146}, Lys^{147}, Phe^{149}, and Ser^{150}) and residues in β9 (Asp^{191}–Val^{196}) showed chemical shift perturbations, suggesting a potential regulatory role by the C-terminal tail. Long range NOEs were observed between methyl protons and residues on the αD helix and C-terminal extension residues such as Leu^{341}, Val^{343}, and Val^{344} (Fig. 2*C*). Our NMR structure reveals that Ala^{201} and Tyr^{202} are located near Thr^{353}, Ile^{354}, Thr^{355}, and Lys^{356}. This is also directly supported by the presence of long range NOEs between the ring protons of Tyr^{202} and Thr^{353}/Thr^{355} (Fig. 2*D*). Fig. 2*B* shows the mapping of the interacting residues. These results suggest the molecular basis of VRK1 activation which requires the molecular interaction between the C-terminal tail and catalytic core of the enzyme. Thus, to delineate further the potential activation mechanism of VRK1, we constructed a series of truncation mutants of VRK1 and examined their characteristics (Fig. 3). Truncation of 75 residues from the C terminus (VRK1$_{1-321}$) causes the mutant VRK1 to become insoluble when expressed in bacterial cells (data not shown). Interestingly, VRK1$_{1-331}$ is soluble but inactive. VRK1$_{1-351}$ and VRK1$_{1-341}$, which lack the C-terminal 45 and 55 residues, respectively, are soluble but show marginal kinase activities. We also evaluated the VRK1 catalytic activity by designing multiple point mutations in the C-terminal tail region. Our data showed that S342A and T353A mutants reduce the autocatalytic activities of VRK1, indicating that those residues play key roles in the kinase activity (supplemental Fig. S3). Taken together, these data suggest that the C-terminal region (residues 321–361) is important for VRK1 physical property as well as its catalysis (Fig. 3) and also support the hypothesis that the C-terminal tail of VRK1 interacts with the catalytic core of the enzyme and plays essential roles for VRK1 activation.

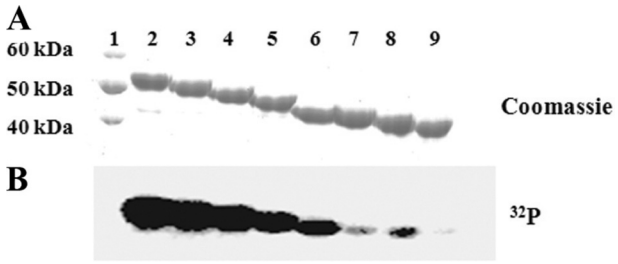

FIGURE 3. **Comparison of autophosphorylation activity of the wild-type and C-terminal truncation mutants of human VRK1.** *A*, the wild-type human VRK1 and C-terminal truncated VRK1 mutants have been purified as described under "Experimental Procedures" and subjected to autocatalytic reactions. *B*, the comparison of autocatalytic activity of the wild-type and the mutant proteins reveals that the C-terminal extension is essential for the kinase activity. *Lane 1*, molecular mass marker; *lane 2*, wild-type VRK1; *lane 3*, VRK1$_{1-391}$; *lane 4*, VRK1$_{1-381}$; *lane 5*; VRK1$_{1-371}$; *lane 6*, VRK1$_{1-361}$; *lane 7*, VRK1$_{1-351}$; *lane 8*, VRK1$_{1-341}$; *lane 9*, VRK1$_{1-331}$.

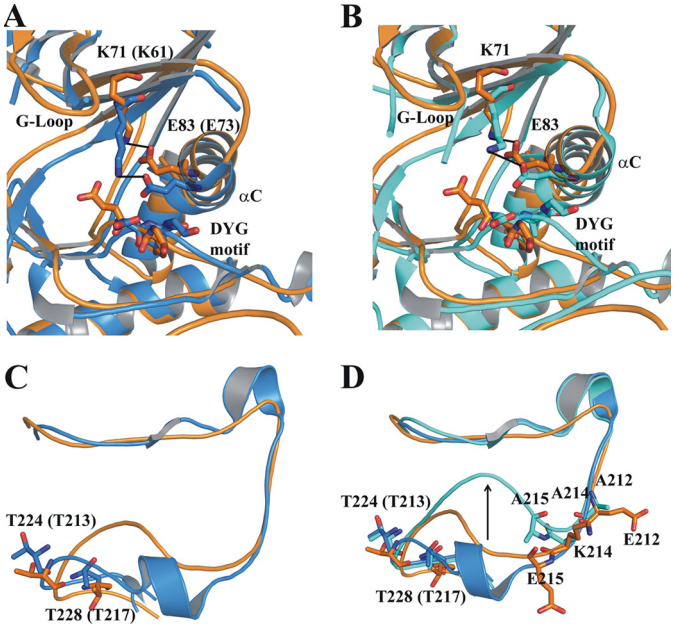

FIGURE 4. **Structural comparison of VRK1 solution structure with other VRK family members.** *A*, superimposition of N-lobes of VRK1 and VRK2 showing the key ion pairing between lysine (β3) and glutamate (αC) residues. VRK1 structure is shown in *orange* and VRK2 in *blue*. Key residues are highlighted with *sticks*, and hydrogen bonds are highlighted with *lines*. *B*, comparison of VRK1 NMR structure ion pairing pattern with VRK1 crystal structure. VRK1 NMR structure is represented in *orange* and VRK1 crystal structure is (PDB 3OP5) highlighted in *cyan*. *C*, structural alignment and comparison of the activation loops of VRK1 and VRK2 with conserved threonine residues highlighted as *sticks*. *D*, superimposition of the activation loops of VRK1 NMR, VRK1 crystal, and VRK2 structures. Residues that are mutated in the activation loop of VRK1 crystal structure (PDB 3OP5) are highlighted with *sticks*. The conformational differences in the activation loop of VRK1crystal structure with respect to VRK2 are shown with an *arrow*.

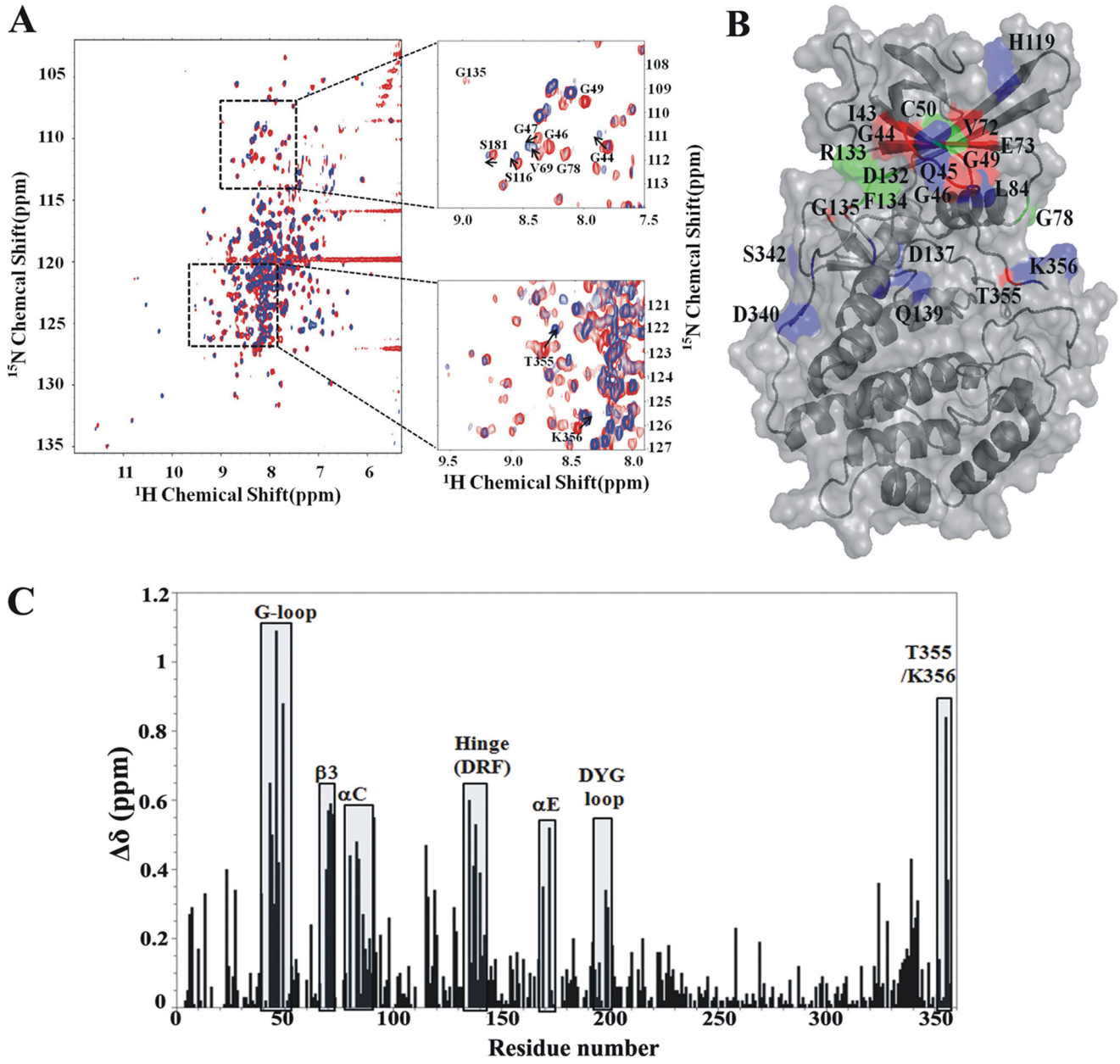

FIGURE 5. **Interaction between ATP analog AMP-PCP and VRK1.** *A*, overlay of ^{1}H-^{15}N TROSY-HSQC spectra of uniformly ^{15}N-labeled VRK1 (*red*) and VRK1 in the presence of AMP-PCP (*blue*) at molar ratio of 1 (VRK1) to 5 (AMP-PCP). Expanded views of chemical shift perturbations upon ligand binding are shown on the *right side* of the panel. The perturbations of chemical shifts from free VRK1 (*red*) to AMP-PCP complex (*blue*) are displayed by *arrows*, and perturbed residues are labeled with a *single letter*. *B*, mapping of ATP binding site and interaction residues on VRK1 based on ^{1}H-^{15}N TROSY-HSQC titration data with AMP-PCP. Perturbed amino acids were displayed according to degree of chemical shift perturbations: *red* ($\Delta\delta > 0.5$), *blue* ($0.3 < \Delta\delta < 0.5$), and *green* (disappeared resonances). The orientation of VRK1 on the *left side* of the panel is the same as that in the Fig. 1, whereas that on the *right side* of the panel is rotated 180° along the *y* axis. *C*, plot of chemical shift perturbations of human VRK1 upon ATP analog AMP-PCP binding. The regions affected by binding of AMP-PCP are shown by a *gray box*, and secondary structure or amino acid residues are *highlighted*.

Structural Comparison of VRK1, VRK Family Members, and Other Kinases—The r.m.s.d. value for 276 C^{α} carbons is 2.56 Å between VRK1 and VRK2 (Fig. 1*C*). Despite the similarity in their structures, they exhibit differences in their local structures. VRK1 is an active member of the VRK family, which encompasses all of the required features/motifs for kinase activity like VRK2. Previous crystallographic studies revealed that VRK3 is having a pseudo-kinase domain with no catalytic ability, unlike VRK1 and VRK2 (22). In the NMR structure of VRK1, αC is rotated inward, a key ion pair between Lys^{71} and Glu^{83} is formed, and the DYG motif (DFG in several other kinases) orients like VRK2 and other active kinases (Fig. 4*A*). The activation loop of VRK1 superimposed well on VRK2, and conserved threonine residues (Thr^{224} and Thr^{228}) also oriented similarly to VRK2 (Fig. 4*C*). The αC4 helix, which is unique in all VRK family members, is also observed in VRK1 and contains the conserved residues Ile^{96}, Trp^{99} forming a hydrophobic interaction with Tyr^{167} in αE, which is similar to what is seen in VRK2 and VRK3 (supplemental Fig. S4). Recently, the VRK1 crystal structure was deposited in the PDB with ID code 3OP5. The crystal structure consists of several mutations in key charged residues and lacking the electron densities for the

C-terminal extension (342–361). Despite the similarity in the overall topology of the kinase domain between our VRK1 NMR structure and the VRK1 crystal structure, several key differences are observed. The distance between ion pairing atoms of Lys^{71} and Glu^{83} is a bit longer in the VRK1 crystal structure than VRK2 and our NMR VRK1 structures. The distance between N^{ϵ} of the lysine and nearest oxygen of carboxyl group present on the glutamate is 2.7, 2.6, and 4.4 Å in the VRK2, VRK1 NMR structure, and VRK1 crystal structure, respectively (Fig. 4, *A* and *B*). Another notable difference is also observed in the activation loop. The center of the activation loop of the VRK1 crystal structure is swung by approximately 8–10 Å compared with VRK2 (C^{α} atom distance between Lys^{218} and Arg^{207} of aligned VRK1 and VRK2, respectively). This difference could be attributable to either several mutations of charged residues (E212A, K214A, and E215A) to alanine in VRK1 crystal structure or might be due to crystal packing with the other chains in the tetramer structure of VRK1 crystal structure (Fig. 4*D*).

The present VRK1 NMR structure was also compared with other kinases with extended C-terminal regulatory tails. Aurora B with INCENP, AMP-activated protein kinase α-subunit with autoinhibitory domain (KD-AID) and p70 ribosomal S6 kinase (p70S6K) crystal structures (PDB ID codes 2BFY, 3H4J, and 3A60, respectively) were employed for comparison purposes (38–40). The C-terminal tail of Aurora B interacts with INCENP and N-lobe of the kinase domain triggering conformational changes in the αC position. This results in an impairment of the key ion pairing between lysine and glutamate residues, leading to the inactivation of the kinase activity (38). In the case of KD-AID, the C-terminal autoinhibitory tail interacts with the N- and C-terminal lobes of the kinase domain from the backside to the hinge region and constrains the mobility of αC helix (39). The autoinhibitory mechanism of p70S6K is not yet clearly established by structural studies. Comparison of VRK1 with these three structures reveals notable differences in the αI helix orientation. In VRK1, αI is relatively straight and long compared with other three kinases and even VRK2. All aforementioned kinases posses a kink in αI which leads the C-terminal tail toward the N-terminal lobe or backside of the hinge region (supplemental Fig. S5, *A–C*). Another important observation made by comparing the sequences of αI is that all three kinases possess a proline residue at the start of the kink, which is replaced by a glutamine residue in VRK1 (supplemental Fig. S5*D*). Moreover, a unique feature of the VRK family structures is the presence of αC4, an additional helix inserted between αC and β4. Although the specific role of αC4 is not clear at this moment, we speculate that it may help the proper orientation of C-terminal tail in VRK1. Superimposition of VRK1 and KD-AID reveals that the autoinhibitory C-terminal tail of KD-AID occupies the position of VRK1 αC4 (supplemental Fig. S5*C*). These differences could be critical to divert the C-terminal tail toward other side of the kinase domain.

Interactions with ATP and AMP-PCP—We have tested the substrate binding properties of VRK1 by performing two-dimensional ^{1}H-^{15}N HSQC titration with AMP-PCP, an ATP analog (Fig. 5*A*). The backbone amides around the ATP binding pocket residues (Ile^{43}, Gly^{46}, Gly^{49}, Val^{70}, Lys^{71}, Val^{72}, and Glu^{73}) displayed the largest chemical shift changes (Fig. 5, *B* and *C*, $\Delta\delta > 0.5$). Residues Gln^{45}, Gly^{47}, and Val^{69}, Leu^{80}, Glu^{83}, and Leu^{84} also showed relatively big chemical shift perturbations (Fig. 5, *B* and *C*, $0.3 < \Delta\delta < 0.5$). These residues are located on the G-loop and β3 and αC. NMR signals of Asp^{132}, Arg^{133}, and Phe^{134} belonging to the DRF motif or hinge region disappeared, and a chemical shift of Gly^{135} also dramatically shifted ($\Delta\delta = 0.6$), indicating that these residues plays an important role during catalysis by interacting with adenosine moiety of ATP molecule. Other spectral changes upon addition of the ATP analog were observed in residues on the DYG motif (Asp^{197}, Tyr^{198}, and Gly^{199}), which interact with the γ-phosphate group of AMP-PCP. NMR signals of Asp^{197} also completely disappeared in the same manner as that observed in residues on DRF motif. Tyr^{198} and Gly^{199} show intermediate chemical shift perturbation ($\Delta\delta \sim 0.3$). The chemical shift perturbation data are consistent with the expected ATP binding site. Moreover, changes were observed in residues Leu^{339}, Asp^{340}, Leu^{341}, and Ser^{342}, which interact with the catalytic core, especially the αD helix. Interestingly, Thr^{355} and Lys^{356} at the C-terminal extension showed chemical shift perturbations, indicating that these residues, especially Thr^{355}, could be related to the ligand binding process. Because Thr^{355} is considered as a potential autophosphorylation site located nearby catalytic and activation loop, it may be important for autocatalytic reaction of VRK1. Taken together, these data suggest that VRK1 may undergo a structural rearrangement induced by ligand binding and cause the changes of dynamic properties of these residues. In conclusion, we report the first NMR solution structure of a catalytically active form of human VRK1 which provides insights into the role of the extended C-terminal tail on its bioactivity. The noncatalytic C-terminal domain of VRK1 (residues 341–361) forms a number of crucial interactions with the catalytic domain, which is critical for structural stability and catalysis. Deletion mutant experiments and their NMR titration analyses also substantiated these observations.

Acknowledgments—We thank Michael Sattler for helpful discussion and a critical review of the manuscript. We also thank the Korea Basic Science Institute and RIKEN for NMR facility access and data acquisitions.

REFERENCES

1. Sánchez-Barrena, M. J., Fujii, H., Angulo, I., Martínez-Ripoll, M., Zhu, J. K., and Albert, A. (2007) *Mol Cell* **26,** 427–435
2. Hunter, T. (1995) *Cell* **80,** 225–236
3. Shchemelinin, I., Sefc, L., and Necas, E. (2006) *Folia Biol.* **52,** 81–100
4. Trevino, S. R., Scholtz, J. M., and Pace, C. N. (2007) *J. Mol. Biol.* **366,** 449–460
5. Bossemeyer, D. (1995) *FEBS Lett.* **369,** 57–61
6. Kornev, A. P., and Taylor, S. S. (2010) *Biochim. Biophys. Acta* **1804,** 440–444
7. Hanks, S. K., and Hunter, T. (1995) *FASEB J.* **9,** 576–596
8. Nichols, R. J., and Traktman, P. (2004) *J. Biol. Chem.* **279,** 7934–7946
9. Traktman, P., Anderson, M. K., and Rempel, R. E. (1989) *J. Biol. Chem.* **264,** 21458–21461
10. Sevilla, A., Santos, C. R., Vega, F. M., and Lazo, P. A. (2004) *J. Biol. Chem.* **279,** 27458–27465
11. Klerkx, E. P., Lazo, P. A., and Askjaer, P. (2009) *Histol. Histopathol.* **24,**

749–759
12. Lopez-Borges, S., and Lazo, P. A. (2000) *Oncogene* **19,** 3656–3664
13. Kang, T. H., Park, D. Y., Kim, W., and Kim, K. T. (2008) *J. Cell Sci.* **121,** 3035–3041
14. Nezu, J., Oku, A., Jones, M. H., and Shimane, M. (1997) *Genomics* **45,** 327–331
15. Nichols, R. J., Wiebe, M. S., and Traktman, P. (2006) *Mol. Biol. Cell* **17,** 2451–2464
16. Gorjánácz, M., Klerkx, E. P., Galy, V., Santarella, R., López-Iglesias, C., Askjaer, P., and Mattaj, I. W. (2007) *EMBO J.* **26,** 132–143
17. Segura-Totten, M., Kowalski, A. K., Craigie, R., and Wilson, K. L. (2002) *J. Cell Biol.* **158,** 475–485
18. Segura-Totten, M., and Wilson, K. L. (2004) *Trends Cell Biol.* **14,** 261–266
19. Lancaster, O. M., Cullen, C. F., and Ohkura, H. (2007) *J. Cell Biol.* **179,** 817–824
20. Kang, T. H., Park, D. Y., Choi, Y. H., Kim, K. J., Yoon, H. S., and Kim, K. T. (2007) *Mol. Cell. Biol.* **27,** 8533–8546
21. Nowak, S. J., and Corces, V. G. (2004) *Trends Genet.* **20,** 214–220
22. Scheeff, E. D., Eswaran, J., Bunkoczi, G., Knapp, S., and Manning, G. (2009) *Structure* **17,** 128–138
23. Pervushin, K., Riek, R., Wider, G., and Wüthrich, K. (1997) *Proc. Natl. Acad. Sci. U.S.A.* **94,** 12366–12371
24. Delaglio, F., Grzesiek, S., Vuister, G. W., Zhu, G., Pfeifer, J., and Bax, A. (1995) *J. Biomol. NMR* **6,** 277–293
25. Goddard, T. D., and Kneller, D. G. (2007) *SPARKY*, version 3, University of California, San Francisco, CA
26. Ruckert, M., and Otting, G. (2000) *J. Am. Chem. Soc.* **122,** 7793–7797
27. Lukin, J. A., Kontaxis, G., Simplaceanu, V., Yuan, Y., Bax, A., and Ho, C. (2003) *Proc. Natl. Acad. Sci. U.S.A.* **100,** 517–520
28. Valafar, H., and Prestegard, J. H. (2004) *J. Mag. Reson.* **167,** 228–241
29. Güntert, P. (2004) *Methods Mol. Biol.* **278,** 353–378
30. Brünger, A. T., Adams, P. D., Clore, G. M., DeLano, W. L., Gros, P., Grosse-Kunstleve, R. W., Jiang, J. S., Kuszewski, J., Nilges, M., Pannu, N. S., Read, R. J., Rice, L. M., Simonson, T., and Warren, G. L. (1998) *Acta Crystallogr. D Biol. Crystallogr.* **54,** 905–921
31. Brunger, A. T. (2007) *Nat. Protoc.* **2,** 2728–2733
32. Shen, Y., Delaglio, F., Cornilescu, G., and Bax, A. (2009) *J. Biomol. NMR* **44,** 213–223
33. Mueller, G. A., Choy, W. Y., Yang, D., Forman-Kay, J. D., Venters, R. A., and Kay, L. E. (2000) *J. Mol. Biol.* **300,** 197–212
34. Koradi, R., Billeter, M., and Wüthrich, K. (1996) *J. Mol. Graph.* **14,** 51–55, 29–32
35. DeLano, W. L. (2002) *The PyMOL Molecular Graphics System*, version 1.3r1, DeLano Scientific, Palo Alto, CA
36. Barcia, R., López-Borges, S., Vega, F. M., and Lazo, P. A. (2002) *Arch. Biochem. Biophys.* **399,** 1–5
37. Laskowski, R. A., Rullmannn, J. A., MacArthur, M. W., Kaptein, R., and Thornton, J. M. (1996) *J. Biomol. NMR* **8,** 477–486
38. Sessa, F., Mapelli, M., Ciferri, C., Tarricone, C., Areces, L. B., Schneider, T. R., Stukenberg, P. T., and Musacchio, A. (2005) *Mol. Cell* **18,** 379–391
39. Sunami, T., Byrne, N., Diehl, R. E., Funabashi, K., Hall, D. L., Ikuta, M., Patel, S. B., Shipman, J. M., Smith, R. F., Takahashi, I., Zugay-Murphy, J., Iwasawa, Y., Lumb, K. J., Munshi, S. K., and Sharma, S. (2010) *J. Biol. Chem.* **285,** 4587–4594
40. Chen, L., Jiao, Z. H., Zheng, L. S., Zhang, Y. Y., Xie, S. T., Wang, Z. X., and Wu, J. W. (2009) *Nature* **459,** 1146–1149